coatings

MDPI

Article

Pitted Corrosion Detection of Thermal Sprayed Metallic Coatings Using Fiber Bragg Grating Sensors

Fodan Deng [1], Ying Huang [1,*], Fardad Azarmi [2] and Yechun Wang [2]

[1] Department of Civil and Environmental Engineering, North Dakota State University, P.O. Box 6050, Fargo, ND 58108, USA; fodan.deng@ndsu.edu

[2] Department of Mechanical Engineering, North Dakota State University, P.O. Box 6050, Fargo, ND 58108, USA; fardad.azarmi@ndsu.edu (F.A.); yechun.wang@ndsu.edu (Y.W.)

* Correspondence: ying.huang@ndsu.edu; Tel.: +1-701-231-7651

Academic Editors: Niteen Jadhav and Andrew J. Vreugdenhil

Received: 30 January 2017; Accepted: 20 February 2017; Published: 24 February 2017

Abstract: Metallic coatings using thermal spraying techniques are widely applied to structural steels to protect infrastructure against corrosion and improve durability of the associated structures for longer service life. The thermal sprayed metallic coatings consisting of various metals, although have higher corrosion resistance, will still corrode in a long run and may also subject to corrosion induced damages such as cracks. Corrosion and the induced damages on the metallic coatings will reduce the effectiveness of the coatings for protection of the structures. Timely repair on these damaged metallic coatings will significantly improve the reliability of protected structures again deterioration. In this paper, an inline detection system for corrosion and crack detection was developed using fiber Bragg (FBG) grating sensors. Experimental results from laboratory accelerated corrosion tests showed that the developed sensing system can quantitatively detect corrosion rate of the coating, corrosion propagations, and cracks initialized in the metallic coating in real time. The developed system can be used for real-time corrosion detection of coated metal structures in field.

Keywords: corrosion detection; thermal spraying metallic coating; fiber Bragg grating; structural health monitoring

1. Introduction

Structural steel is a popular structural material in modern structures such as bridges, buildings, and pipes. With the presence of oxygen and water, steel is prone to corrosion, which is a complex electrochemical process [1,2] and can hardly be prevented. Corrosion on metallic structures can considerably reduce the cross-section area of the associated components and correspondingly lower the capability of carrying loads. This will result in significant impacts on the reliability and safety of the structures which might lead to catastrophic consequence occasionally [3,4].

To protect structural steels from corrosion, coatings are usually applied. Coatings cover the surface of structural steel and change its surface properties, providing a barrel between the steel and the corrosive environments and preventing the presence of water and oxygen to steel. There are two types of coating which are commonly applied in practice, including paints and metallic coatings [5–10]. Paints use layers of soft materials such as polyurethane to block the entrance of water and oxygen [5–7], and some recently developed paints are able to provide sacrificial cathodic protection in addition to the physical blockage [8]. However, due to the low abrasion resistance, paints usually have a limited extension of service life to structures. Thus, when structural steel is in service under aggressive environments, non-ferrous metallic coatings are required instead of or in addition to paints, which are widely applied for corrosion prevention in coastal eras [5,7,9,10].

Metallic coatings predominantly are composed of metal particles have higher corrosion resistance than the substrate material to slow down corrosion process. Other than decelerating the corrosion process, the metallic coatings also improve the wear resistance due to higher hardness and density [7]. To coat non-ferrous metals on structural steels, various coating techniques can be used including hot-dip galvanizing or thermal spraying techniques [11–13]. Hot-dip galvanizing technique usually provides a relatively uniform and thin coating layer with most commonly applied Zinc or aluminum materials. Due to a uniform coating, the quality of the hot-dip galvanizing metallic coatings is generally well controlled [14], but sometimes still subject to cracking issues [15]. While the thermal spraying technique can provide either thin or thick coating with flexible composite coating materials depending on needs to achieve an ultimate corrosion and wear protection. For structural steels servicing in harsh environments, metallic composite coated by thermal spraying technique is commonly used for industrial applications such as pipeline and bridge components [12]. However, thermal spraying technique may have difficulty in guarantee a consistent coating quality. In addition, thermal spray coating powders are usually composed of several different types of metallic particles, adding complexity to the properties and microstructure of the coating [16–18]. In addition, the environment and human factors during coating process can interfere the consistency of coating quality. As a result, even though thermal spray coating promises a longer overall service life for components, the individual component's service life time varies.

To ensure the performance of the thermal sprayed coatings for corrosion and damage protection, non-destructive testing can be applied for coating quality evaluation on requests such as electrochemical method, guided wave, acoustic, ultrasonic, and microwave techniques [19–26]. The application of these techniques requires accessing the structures which may not be the case for some off-shore or marine structures. Thus, an on-site monitoring system for corrosion and crack for thermal sprayed metallic coatings will improve significantly to the safety of the coated structures and further enhance the cost and resource allocation efficiency for potential repair associated and is yet to be developed.

The Fiber Bragg grating (FBG) sensor, due to its high sensitivity, resistance to electromagnetic interference, good durability, low cost, and more importantly capability of real-time monitoring, has become a widely accepted sensing alternative for strain [27–29], temperature [29–31], and possibly crack measurements [32,33] in civil engineering fields. Studies of using FBG sensors in crack detection on concrete and metallic structures had shown that distinguishable data alter could be observed when cracks initiated. Several studies further showed the ability of FBG sensors to locate crack position together with the use of other types of detection methods, such as acoustic emission [34] and ultrasonic sensor system [35]. The advantages of FBG sensor also make it a potential candidate for corrosion monitoring for structures. Lately, several attempts for applying FBG sensor in corrosion of steel rebar in concrete had been made [36–38], demonstrating that noticeable data shift would happen along with the corrosion growth [39,40]. Nevertheless, to date, limited sensing technologies can monitor the corrosion of structural steels with thermal sprayed metallic coatings due to the harsh environment during the thermal spraying process.

In this paper, a corrosion and crack monitoring system for thermal sprayed metallic coatings was developed using embedded FBG sensors. The paper is structured as follows: Section 2 introduces the principle to quantify corrosion rate by the output of embedded FBG sensors and designs the method of embedment of FBG sensors in thermal sprayed metallic coatings; Section 3 provides the setup of proof-of-concept experiments; Section 4 discusses the experimental results with a comparison to visual inspection and electrochemical corrosion rate measurements; and at least Section 5 delivers the conclusions and prospective future work.

2. Operational Principles

The corrosion of a metal is an electrochemical process. Although there are various factors controlling the process of corrosion, including the physical and chemical properties of metal,

the roughness of metal surface, temperature, etc., it is clear that presence of both water and oxygen is necessary for electrochemical reaction of corrosion to occur. With the presence of free electrons, water and oxygen, reduction happens at cathodes, as shown in the reaction below [3,41]:

$$2H_2O + O_2 + 4e^- = 4OH^- \quad (1)$$

Reduction at cathodes will introduce a material property change of the cathodes, for instance, for steel material, the iron will change to oxidized iron with size ten times larger the original iron particles. Thus, detecting the material volume or expansion change using sensing techniques throughout the corrosion process can potentially reveal the corrosion mechanism of the electrochemical process of metals.

2.1. Principle of FBG Sensor

In this paper, a FBG sensor will be used to detect the corrosion and crack initiation in thermal sprayed metallic coatings. Figure 1 shows a typical structure of a FBG sensor. It is fabricated by periodic heating of fiber core using high-power UV laser, inducing a periodic modulation of the core refractive index. With the modulation, if a broadband light beam is transmitted through the FBG, part of the incoming light with certain wavelength will be reflected showing a dip in the reflected light spectrum, known as Bragg wavelength (λ_B). The Bragg wavelength needs to meet the Bragg condition with effective refractive index (n_{eff}) and grating pitch (Λ), as [42]:

$$\lambda_B = 2n_{eff} \cdot \Lambda \quad (2)$$

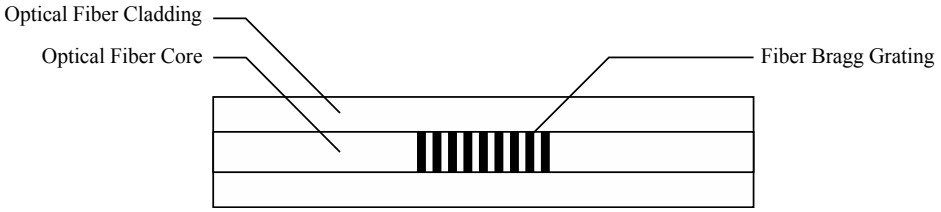

Figure 1. The structure of a typical FBG sensor.

The effective refractive index (n_{eff}) is determined by the transmitting media, which is optical fiber core in the case of a FBG. It will not change as there is no material change related to optical fiber core during its use. However, the grating pitch (Λ) does change with length variation of FBG, whether it is caused by a temperature raise/drop (ΔT) or an external tension/compression (ε_c). This will result in a shift in Bragg wavelength. From the wavelength spectrum of reflected light, a shift in peak wavelength can be found as shown in Figure 2. The amount of Bragg wavelength change with strains or temperatures can be calculated as below [42]:

$$\frac{\Delta\lambda_B}{\lambda_B} = (1 - P_e) \cdot \varepsilon_c + [(1 - P_e) \cdot \alpha + \xi] \cdot \Delta T \quad (3)$$

where P_e is the photoelastic constant of the fiber and α is the thermal expansion coefficient of the fiber, both determined by the material of fiber. The temperature effects in Equation (2) could be eliminated by applying a reference sensor.

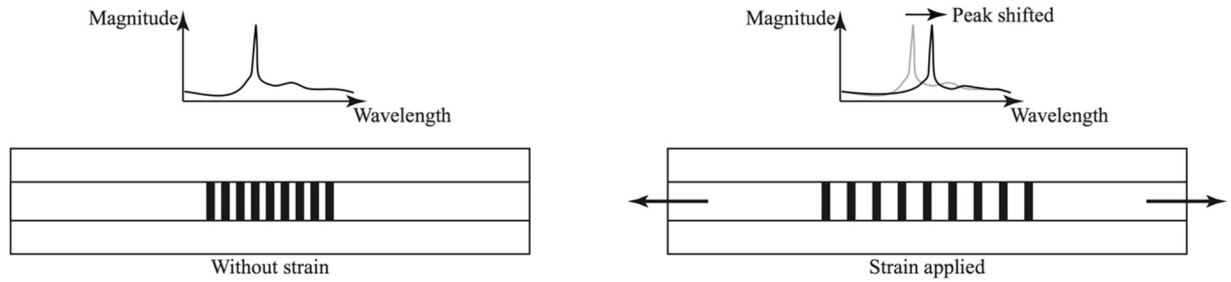

Figure 2. Bragg wavelength shift of reflected light when strain is applied on FBG sensor.

If the Bragg wavelength of temperature reference sensor is λ_{ref}, then the wavelength change induced by external strain can be described as:

$$\frac{\Delta\lambda_B}{\lambda_B} = (1 - P_e)\cdot\varepsilon_c + \frac{\Delta\lambda_{ref}}{\lambda_{ref}} \quad (4)$$

If a reference sensor is selected with $\lambda_{ref} \approx \lambda_B$, the wavelength change after elimination of temperature effects ($\Delta\lambda = \Delta\lambda_B - \Delta\lambda_{ref}$) can be expressed as:

$$\Delta\lambda = \Delta\lambda_B - \Delta\lambda_{ref} = (1 - P_e)\cdot\lambda_B\cdot\varepsilon_c \quad (5)$$

Hence, with the measurement of Bragg wavelength change of a test sensor and a reference sensor, the strain on a FBG can be calculated, which may further relate to corrosion and crack progressing status.

2.2. Operational Principle of the Corrosion and Crack Sensing in Coatings Using Embedded FBG Sensors

To monitor corrosion and cracks in the thermal sprayed metallic coatings, it is required to embed the FBG sensor inside the coating. When embedded, the coating acts as constrains to the FBG sensor with an initial strain, ε_0, introducing an initial Bragg wavelength of, λ_0. If no corrosion or crack occurs, the Bragg wavelength will only vary with surrounding temperature. With a temperature reference FBG sensor on site, no Bragg wavelength change of the test sensor is expected based on Equation (4). However, when corrosion occurs in the steel substrate or in the metallic coatings, as shown in Figure 3, the corrosion products will push the coating up, inducing a strain on the FBG sensor, as ε_i, that can be monitored by the Bragg wavelength change of the FBG sensors, as λ_i, where i is corrosion time step.

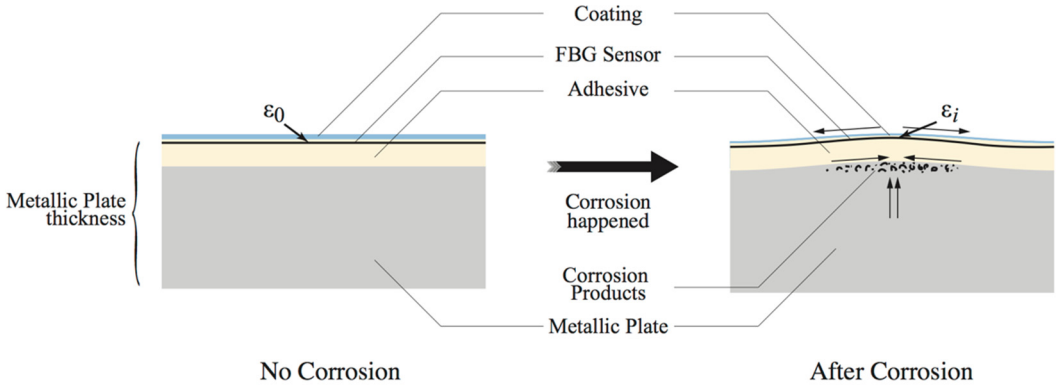

Figure 3. Cross-section of corrosion monitoring system.

To simplify the structure for analysis, if the FBG sensor is packaged using steel tubes or similar for protection, the corrosion induced strain to the constrained FBG sensor inside coating and adhesive

if any during embedment, can be analyzed using a simply supported beam theory. Two assumptions are made based on a typical corrosion:

- The corrosion analyzed in this paper is pitted (localized) corrosion so its corrosion production is accumulated within a relatively small area comparing to the total span of the packaged FBG sensor;
- The expansion of corrosion productions mainly occurs in vertical direction.

As shown in Figure 4, with Assumption (a), the corrosion product expansion can be simulated as a point load, F, induced displacement, Δ, in the middle of the FBG sensor as the coating detaching away from the steel substrate due to the presence of corrosion products and at the same time other coatings remain attaching to the steel substrate.

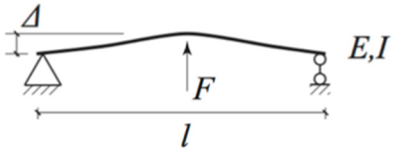

Figure 4. Simple supported beam system with a displacement in the middle.

Thus, the corrosion induced strain monitored by the embedded FBG sensor, ε_i, and the displacement in the middle of the total span, Δ, can be calculated as:

$$\varepsilon_i = \frac{\sigma}{E} = \frac{My}{EI} = \frac{ly}{2EI} \cdot F \tag{6}$$

$$\Delta = \frac{Fl^3}{48EI} = \frac{l^3}{48EI} \cdot F \tag{7}$$

where σ is the normal stress at a distance y from the neutral surface of bending, M is the resistance moment of the section at middle span, E is the Young's modulus of adhesive, I is the moment of inertia, l is the span of beam, y is half of the height of cross-section, and F is the induced concentrated force by corrosion at the middle of total span. Let $k_1 = ly/(2EI)$ and $k_2 = l^3/(48EI)$. Then the relation between the center displacement (Δ) to that of the strain in the embedded FBG sensor (ε_i) can be expressed as:

$$\varepsilon_i = k_1 \cdot F = \frac{k_1}{k_2} \cdot \Delta \tag{8}$$

With Assumption (b), the total volume of corrosion products, V, would be linear proportional to the corrosion induced center displacement on the FBG sensor (as volume increased linearly corresponding to the increase in height), which can be described as:

$$V = k_3 \cdot \Delta = \left(\frac{k_2 k_3}{k_1} \right) \cdot \varepsilon_i \tag{9}$$

where k_3 is the linear scaling factor between volume of corrosion products and induced center displacement.

As described in the definition, the corrosion rate (CR) of a metal is the derivative of the total lost weight of metal (m) due to corrosion with respect to time (t), and the weight is the product of the density of metal (ρ) and volume (V'). When the type of metal is determined, the density of metal and the expansion factor (k_4) between volume of corrosion products (V), and lost volume of metal due to corrosion (V'), are constants. Hence, with Equation (8), the relationship between corrosion rate and strain monitored by the embedded FBG sensor can be drawn as below:

$$\mathrm{CR} = \frac{\mathrm{d}m}{\mathrm{d}t} = \rho \frac{\mathrm{d}V'}{\mathrm{d}t} = \rho k_4 \frac{\mathrm{d}V}{\mathrm{d}t} = \frac{\rho k_2 k_3 k_4}{k_1} \cdot \frac{\mathrm{d}\varepsilon_i}{\mathrm{d}t} \tag{10}$$

Combing Equations (4)–(9), the monitoring of the Bragg wavelength changes of the embedded FBG sensors can then be related to the corrosion rate of the thermal sprayed coatings or the coated subtracts as below:

$$\mathrm{CR} = \frac{\rho k_2 k_3 k_4}{\lambda_B k_1 (1 - P_e)} \cdot \frac{\mathrm{d}\Delta\lambda}{\mathrm{d}t} = \alpha \cdot \frac{\mathrm{d}\Delta\lambda}{\mathrm{d}t} \tag{11}$$

where CR is the corrosion rate, $\Delta\lambda$ is the Bragg wavelength change measured by the embedded FBG sensor, and α is the sensitivity of the sensor toward corrosion rate of metals which can be calibrated with known corrosion rate of one certain material.

With laboratory accelerated corrosion tests, the parameters in Equation (10) can be calibrated. The calibrated model can then be applied to various thermal sprayed coatings in field for corrosion monitoring of coated steel structures. More importantly, as corrosion further develops, cracks will be initialized inside coating resulting in coating breakages, which will release the induced constrain of FBG sensors and change the boundary conditions of the FBG sensor for existing corrosion products. The lift-up phenomenon mentioned above will disappear, resulting in a sudden drop in Bragg wavelength of FBG sensors, which can be notified and used to monitor the cracks on thermal spayed metallic coatings.

2.3. Sensor Design

The sensor system is designed to follow the operational principles discussed above and at same time to protect the sensor from the harsh environments during thermal spaying coating process. In this paper, the bare FBG sensor (OS 1100 Fiber Bragg Grating sensors from Micron Optics Inc., Atlanta, GA, USA) is packaged using steel hypodermic tube and attached to the surface of steel substrate using adhesives before embedment inside the thermal spraying coatings. Two types of hypodermic tubes are used to secure FBG sensor and the communication fiber. Figure 5a–d show the packaging process of the sensor. The hypodermic tube used to protect the FBG sensing unit has an inner diameter of 0.01225 inch as shown in Figure 5a. M-Bond 200 epoxy is used to attach the sensing unit to the hypodermic tube as shown in Figure 5b. The hypodermic tube to protect the communication fiber has an inner diameter of 0.028 inches as shown in Figure 5c. In order to provide a comprehensive protection for the FBG strain sensor, two types of hypodermic tubes overlap with each other by a quarter inch, as shown in Figure 5d. Overlap section of two types of tubes is ensured by applying M-Bond 200 epoxy to prevent sliding.

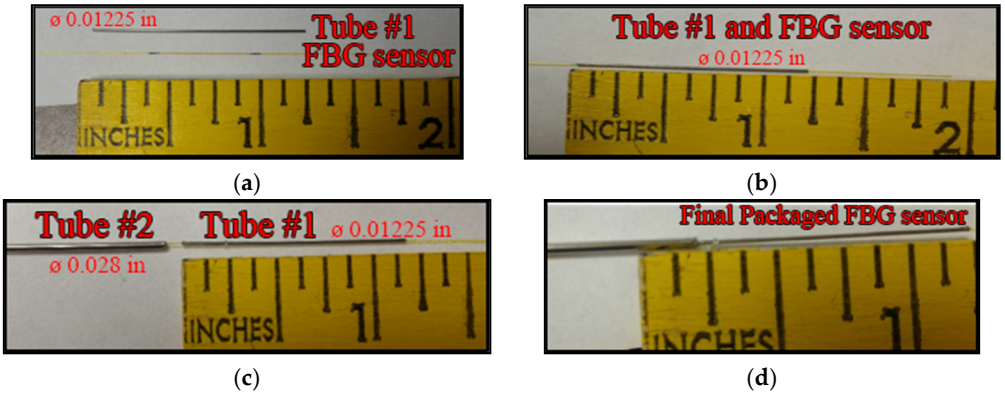

Figure 5. FBG sensor packaging. (**a**) FBG sensor and packaging tube; (**b**) FBG sensor in packaging tube; (**c**) Communication fiber protection tube; (**d**) Connection between two tubes.

The packaged FBG sensors then are attached to the steel substrate using adhesive as shown in Figure 6a. The adhesives used in this study is metallic-stainless steel based adhesive (Durabond™ 954 from Cotronics Corp., Brooklyn, NY, USA), due to its high wear, abrasion, and hear resistance. Protected by the packaging and the adhesive, metallic coatings are then thermally sprayed on top of the sensor.

To test the worst-case scenario and ensure the embedment of FBG sensor can survive most thermal spraying techniques, in this paper, the High Velocity Oxygen Fuel (HVOF) thermal spraying technique is selected and applied to introduce the metallic coating, due to the fact that the HVOF technique introduces the harshest environment for FBG sensor embedment. The HVOF thermal spraying technique generates high velocity carrier gas by combusting the mixture of oxygen and fuel gas. The coating metallic powder particles mixed with carrier gas are injected onto the desired pre-treated substrate surface through a spray gun [5]. The high temperature and high velocity of carrier gas stream contributes to the forming of a dense, adhesive, less porous, long-lasting, and high corrosion and wear resistive hard coating. Due to the high temperature and high velocity gas stream, the HVOF thermal spraying also generates an extremely harsh environment for the embedment of FBG sensors. The developed sensor embedment technique has been approved to be sufficient protecting against the harsh environments introduced by the HVOF thermal spraying process. Figure 6b shows an example coated steel plate with embedded FBG sensors after surviving HVOF thermal spraying process.

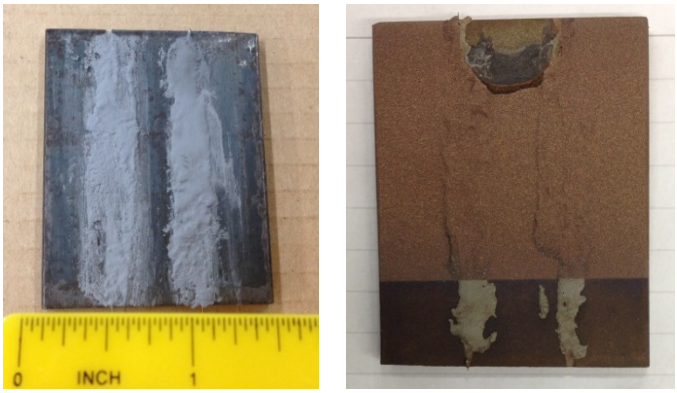

(**a**) (**b**)

Figure 6. Example samples with attached FBG sensors (**a**) before and (**b**) after metallic coatings.

Figure 7 shows the monitored Bragg wavelength changes of one FBG sensor during the HVOF thermal spraying coating process. It can be seen that during the HVOF thermal spraying process, the Bragg wavelength increased significantly from 1583.89 to 1584.68 nm, indicating an 83.2 °C temperature increase (temperature sensitivity of FBG sensor: 9.5 pm/°C) on the surface of the coated sample. In addition, several segments of the curve can be distinguished by an increase followed by a decrease in Bragg wavelength, which reflect different HVOF thermal spraying cycles. A total number of 6 spraying cycles can be found in the following figure.

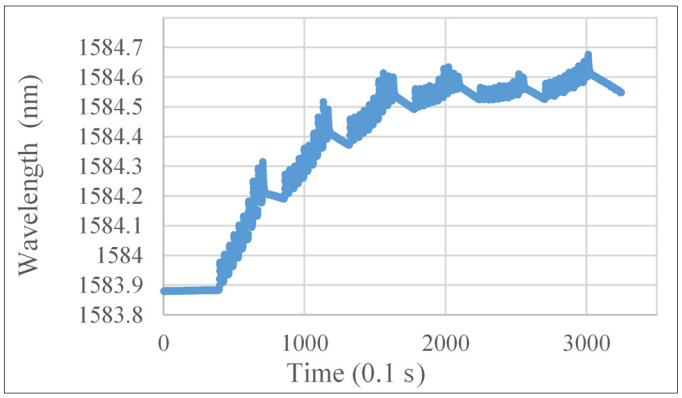

Figure 7. Monitored Bragg wavelength changes of a FBG sensor during thermal spraying coating process.

3. Experimental Section

3.1. Sample Preparation

To validate that the developed embedded FBG sensor system can monitor the corrosion and cracks in the metallic coatings, four steel plate samples (Samples #1–#4) were prepared following the procedure discussed above in addition to two coating control samples without embedded sensors (Samples #5 and #6) and one sensor control sample with sensor but no coating (Sample #7). Figure 8 shows the four samples with embedded sensors before coating. All the FBG sensors were embedded on the top portion of the steel plates.

With the samples prepared, samples #1–#6 were coated using the HVOF thermal spray coating process by applying Al-Bronze composite material (Diamalloy™ 1004, Oerlikon Metco, Winterthur, Switzerland, Cu-9.5-Al-1-Fe). An automatic robotic spraying arm with spraying gun was applied during coting process to ensure a uniform coating on the substrate as shown in Figure 9a. The speed of the movement and the total numbers of spraying rounds can be controlled for specific coating requirements. Sample #5 was used to test the mechanical property of the thermal sprayed composite coating and Sample #6 was used to obtain SEM analysis for the cross-section of the coating quality control as shown in Figure 9b. The metallic coating was applied densely and uniformly on top of the embedded sensor with a thickness of 90 μm from the SEM image of the coating in Figure 9b. Knoop Micro indentation hardness test is used to measure hardness of coating materials as also shown in Figure 9b. The hardness test was carried out on the coating cross section according to ASTM E384-11 using CLARK CM-800AT (Sun-Tec Corp., Novi, MI, USA). The average hardness of the thermally sprayed Cu-Al-Bronze coating was estimated near 139.4 HK (≈125 Hv) from 10 hardness measurement.

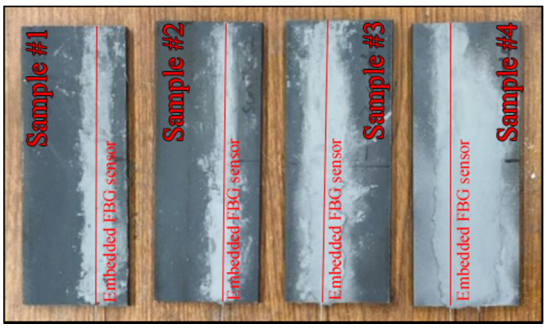

Figure 8. Embedded FBG sensors in steel plates.

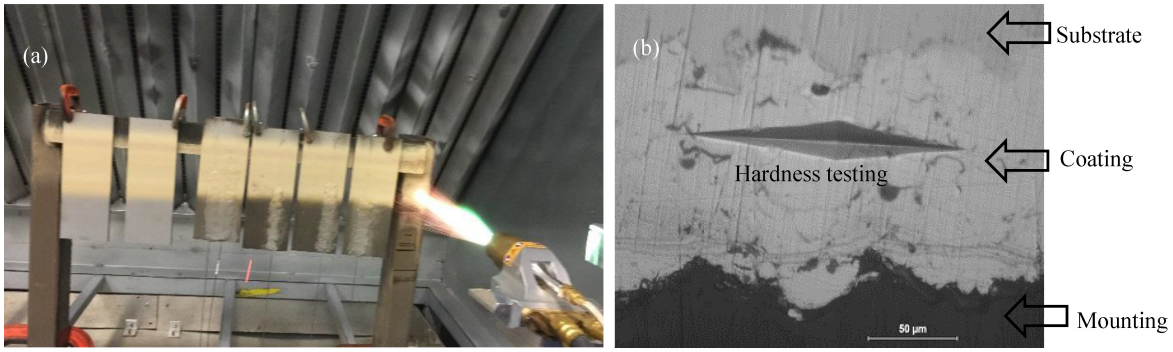

Figure 9. (**a**) HVOF thermal spray coating application and (**b**) SEM image of the coating.

3.2. Corrosion Rate Measurement Using Electrochemical Approach

Accelerated corrosion tests were performed on Sample #1–#4 and Sample #7 using the embedded sensing systems. To compare with traditional sensing technology for corrosion measurements,

electrochemical method for corrosion rate estimation was performed on one coated sample with embedded sensors, Sample #4 before the accelerated corrosion tests to obtain a reference corrosion rate. A Gamry Reference 600 Ptentiostat/Galvanostat/ZRA (Gamry, Warminster, PA, USA) was used in this study to perform the electrochemical tests. Figure 10 shows the experimental setup using the electrochemical approach. A scan rate was set to be 0.1 mV/s and the scan range was set to be ±250 mV vs. corrosion potential.

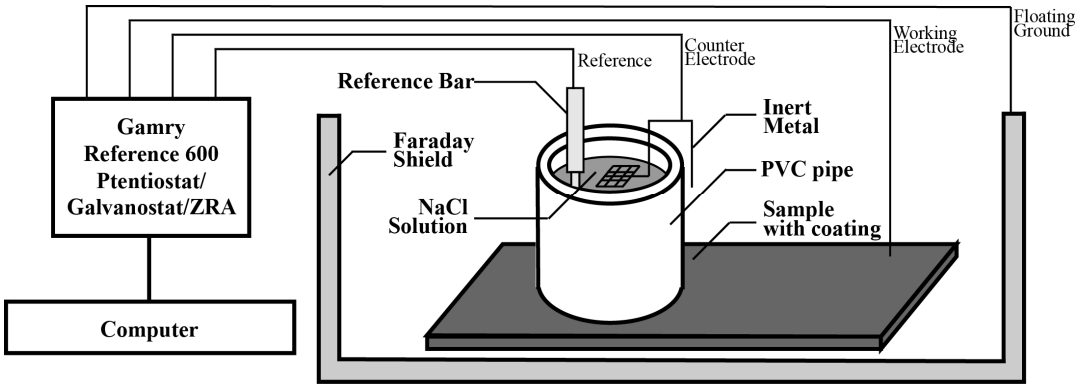

Figure 10. Experimental setup for electrochemical tests.

3.3. Experimental Setup for Accelerated Corrosion Test

Accelerated corrosion tests were then performed on the coated and uncoated samples with embedded sensors (Samples #1–#4 and #7) as shown in Figure 11 for test setup. To create a corrosive environment for accelerated corrosion, a PVC tube was attached on top of the sample with embedded sensors and filled with 3.5 wt % sodium chloride (NaCl) solution. The experiments run for 6 days. The Bragg wavelength changes of samples with embedded sensors had been recorded using optical signal analyzer (National Instruments PXIe-4844 Optical Sensor Interrogator integrated with PXIe-1071 Controller and PXIe-8133 Chassis, National Instruments, Austin, TX, USA) continuously for the 6 days with a sampling frequency of 10 Hz. Visual inspections for all the samples were also scheduled at 12:00 p.m. daily for identifying the existence of corrosion on surface of the samples.

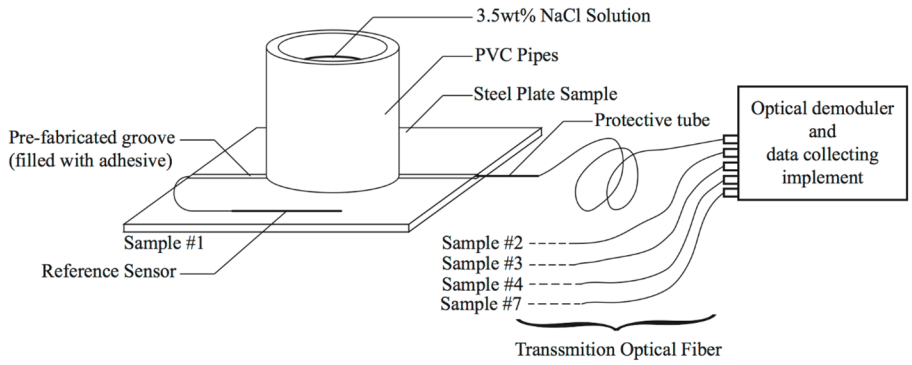

Figure 11. Accelerated corrosion test set-up.

4. Experimental Results and Discussion

4.1. Experimental Results from Electrochemical Method

Figure 12 shows the result from the electrochemical method of Sample #4 before the accelerated corrosion tests using embedded sensors. The corrosion rate of the thermal sprayed composite coating, CR, can be estimated from Figure 12 using the equation as follow [43]:

$$\mathrm{CR} = \frac{\beta_A \cdot \beta_C}{2.3 R_P (\beta_A + \beta_C)} \cdot \frac{K \cdot \mathrm{EW}}{d \cdot A} \tag{12}$$

where β_A and β_C are the Tafel constants, R_P is the polarization resistance of the material, K is unit conversion factor, EW is the equivalent weight of tested material, d is density of tested material, and A is the testing area. Table 1 listed all the estimated parameters in Equation (11) from Figure 12 for the thermal sprayed composite coating of Sample #4. The measured corrosion rate of the metallic coating produced by the electrochemical method is 0.5054 mil/year.

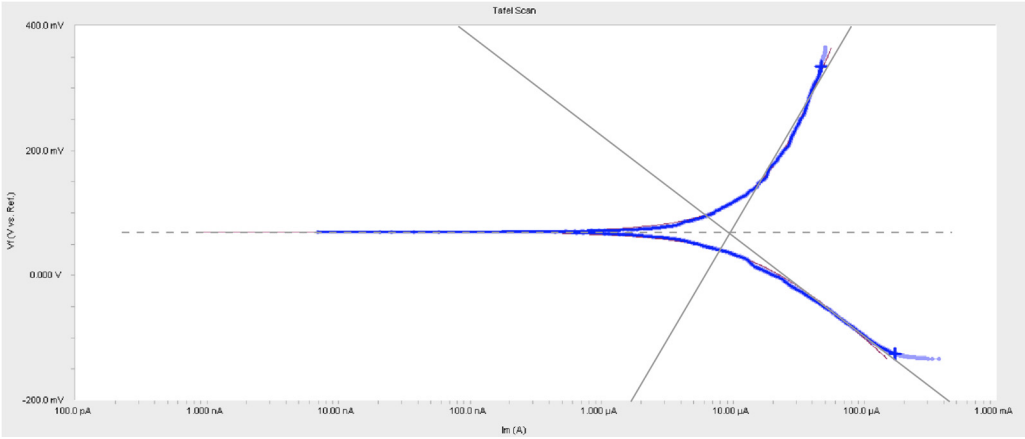

Figure 12. Tafel plot measurement result of Sample #4.

Table 1. Tafel plot measurement details of Sample #4.

Sample Number	Anodic Tafel Constant, βa, (V/Decade)	Cathodic Tafel Constant, βa, (V/Decade)	Polarization Resistance (kΩ)	Corrosion Current (amps)	Corrosion Rate (mil/Year)
Sample #4	0.5348	0.2047	2.3	2.798×10^{-5}	0.5054

4.2. Experimental Results from Accelerated Corrosion Tests Using Embedded FBG Sensors

Figure 13 shows the test results of Bragg wavelength changes with test time obtained from the embedded FBG sensors for all the five samples (Samples #1–#4 and #7) after compensating temperature as the corrosion on the surface of the samples progressing in days. It can be seen from Figure 13 that the sensor reading for different materials varies significantly. The sensor reading from Sample #7 for bare steel showed significant difference when compared to that from Samples #1–#4 for thermal sprayed composite metallic coatings. In addition, it can be seen that the readings from Sample #2 and Sample #7 follow similar trends that the Bragg wavelength increased rapidly in first three days and kept mostly steady thereafter. While Samples #1, #3, and #4 showed a stable Bragg wavelength changes in the first 3 days, and exhibit different patterns after the 3rd day. The Bragg wavelength change of Sample #1 started to increase after the 3rd day. The Bragg wavelength of Sample #3 continued to stay similar range as the previous three days, however, that of Sample #4 dropped dramatically at the end of the 4th day.

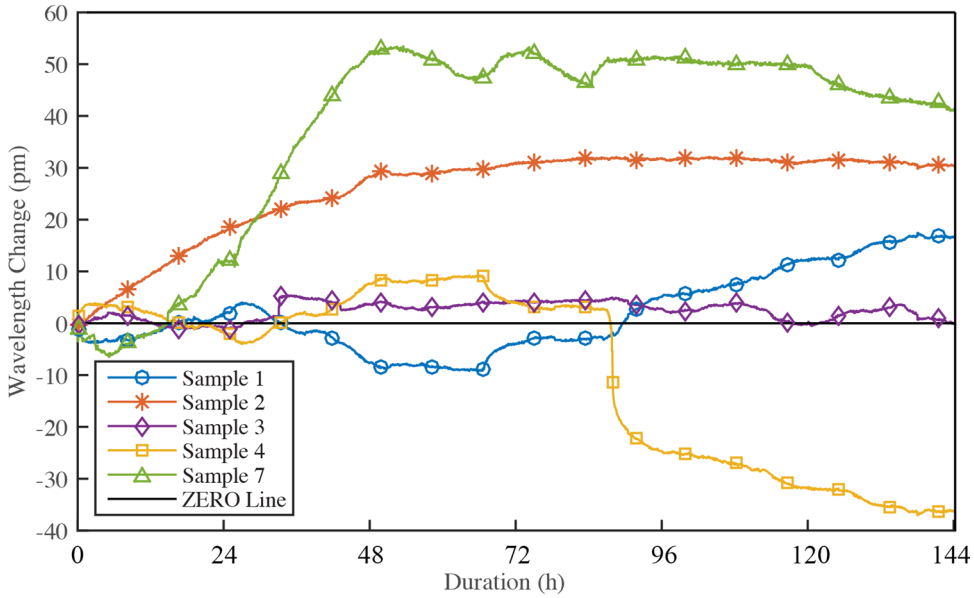

Figure 13. Temperature compensated Bragg wavelength changes of embedded FBG sensors with test time.

To explain these observations, we recorded the visual inspection of all the samples for the six days at 12:00 p.m. each day. Figures 14–18 show the visual inspection of each sample during the test period at Day 1, Day 2, Day 3 or Day 4, and Day 6, respectively. It is worth noting that the corrosion initialized at different days for each sample. The pitted corrosion on top of the embedded sensor of Sample #1 started on the Day 3 of testing as in Figure 14, which is very consistent with the recorded FBG sensor readings as shown in Figure 13 for Sample #1. The pitted corrosion on top of the embedded sensor of Sample #2 started on Day 1 right after the samples in solution as shown in Figure 14. This observation also corresponds well with the continuous changes of Bragg wavelength of the FBG sensor during the process as shown in Figure 13 of Sample #2. For Sample #3, although some pitted corrosion occurs, no corrosion is initialized on top of the sensor throughout the testing as seen in Figure 16. In Figure 13 for Sample #3, the Bragg wavelength of the embedded FBG sensor stays almost the same all the way to the end of the test, which matches well with the observations from visual inspection. For Sample #4, the sample already showed a serious corrosion obtained from the electrochemical measurement approach before the accelerated corrosion tests. Around Day 4 of testing, noticeable coating breakage can be observed through visual inspection as seen in Figure 17c, which also can be clearly identified in Figure 13 of Sample 4. For Sample #7, the corrosion starts on Day 2 as observed from Figure 18, which also matches well with Figure 13 qualitatively. To qualitatively measure the corrosion rate from the FBG readings, more discussions and future data correlation between sensor readings and corrosion performance are presented in next section.

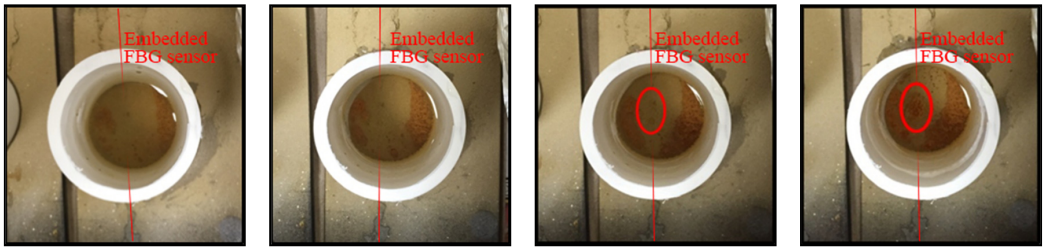

(**a**) (**b**) (**c**) (**d**)

Figure 14. Visual inspections of Sample #1. (**a**) Day 1; (**b**) Day 2; (**c**) Day 3; (**d**) Day 6.

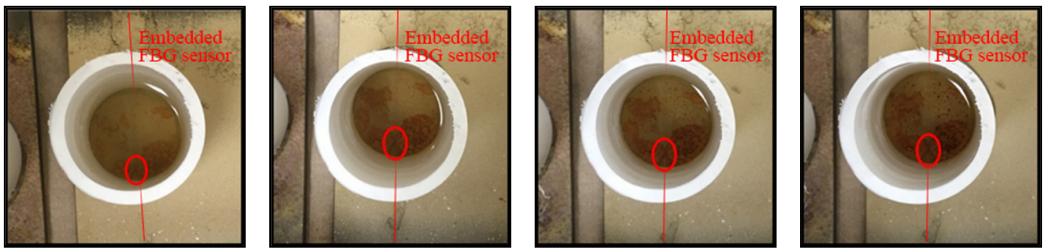

(**a**) (**b**) (**c**) (**d**)

Figure 15. Visual inspections of Sample #2. (**a**) Day 1; (**b**) Day 2; (**c**) Day 3; (**d**) Day 6.

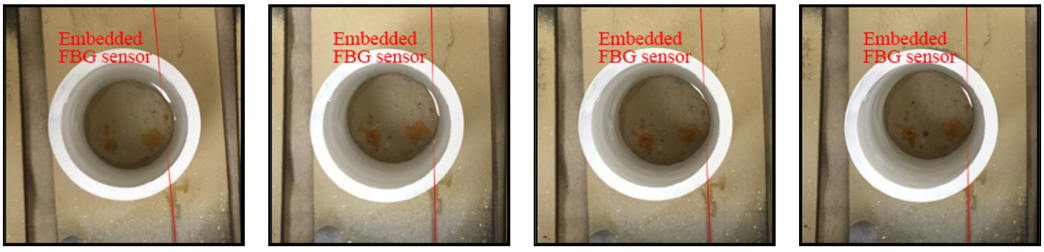

(**a**) (**b**) (**c**) (**d**)

Figure 16. Visual inspections of Sample #3. (**a**) Day 1; (**b**) Day 2; (**c**) Day 3; (**d**) Day 6.

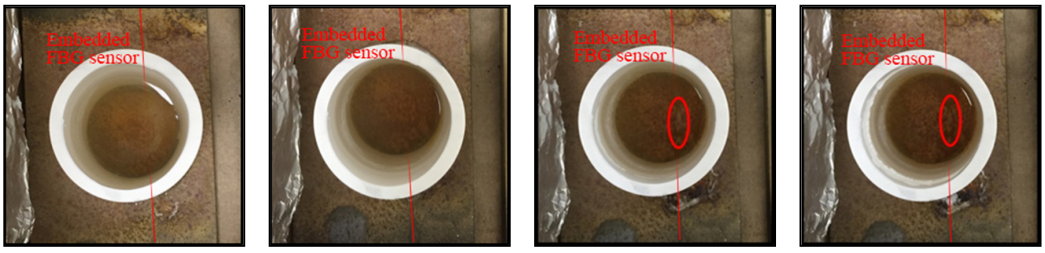

(**a**) (**b**) (**c**) (**d**)

Figure 17. Visual inspections of Sample #4. (**a**) Day 1; (**b**) Day 2; (**c**) Day 3; (**d**) Day 6.

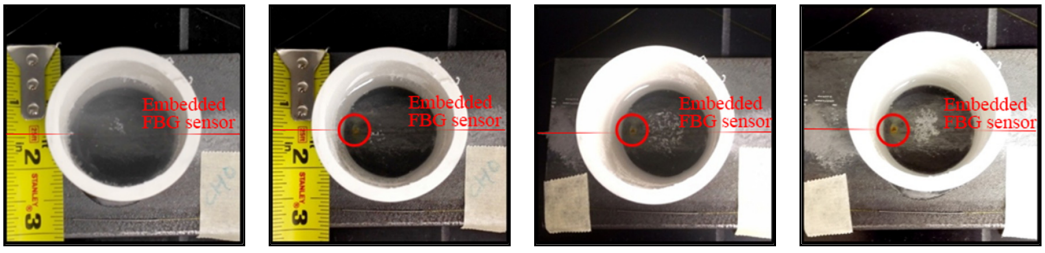

(**a**) (**b**) (**c**) (**d**)

Figure 18. Visual inspections of Sample #7. (**a**) Day 1; (**b**) Day 2; (**c**) Day 3; (**d**) Day 6.

4.3. Discussion and Data Analysis

To further analyze the data from the embedded FBG sensors for quantitative corrosion and crack measurements, we take a close look for Samples #1, #2, and #7 as in Figure 19, since these three samples showed similar data pattern of a three-phase phenomenon as seen in Figure 13. The observations of various phases of corrosion process for metals are consistent with that from previous researches performed by Melchers et al. in 2005 [4]. Melchers et al. proposed that in the early stage of metal corrosion process, the corrosion performance in sea water (close to 3.5% NaCl solution as in our lab tests) can be described as a multi-phase corrosion time model based on extensive field experiments

25. The three main early phases include: (1) Phase 0, the phase of short-term influences; (2) Phase 1, the phase of high corrosion rate; (3) Phase 2, the phase of stabilized corrosion progress. From Figure 19, it can be clearly seen that the embedded FBG sensor successfully discovered the phases of the corrosion process of the thermal sprayed coatings.

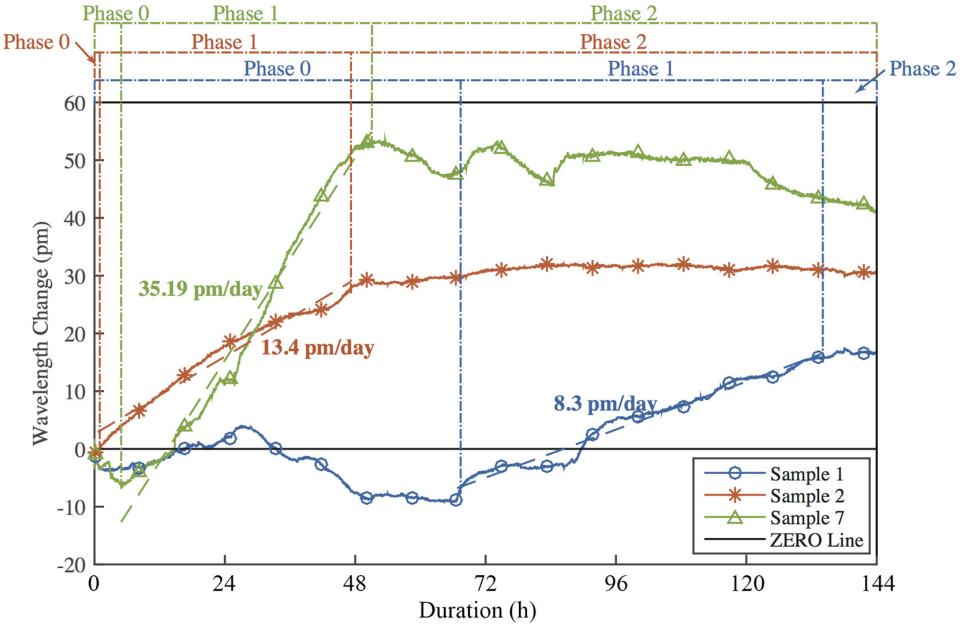

Figure 19. Bragg wavelength change vs. time of Samples #1, #2, and #7 for data analysis.

Detail observations of each phase identified by the embedded FBG sensors on the three samples (#1, #2, and #7) are further discussed as follows:

- In Phase 0 (short-term influences phase), the corrosion is initialized and corrosion products start to fill the pores between adhesive and the FBG sensors. As a result, compression strains are observed on FBG sensors, introducing a drop of Bragg wavelengths of all FBG sensors on all three samples shown in Figure 19.
- In Phase 1 (high corrosion rate phase), oxygen surrounded at corrosion area is consumed and more oxygen is rapidly absorbed in water, which results in high corrosion rate of the material. Due to principles discussed in Section 2, corrosion products tend to lift the embedded FBG sensors as a simply supported beam, causing an increase in Bragg wavelengths following Equations (3)–(5) in Section 2. Thus, the slope of Bragg wavelength change in Phase 1 reflects the production rate of corrosion products, which is the expected corrosion rate in Equation (6). Sample #7 with bare steel has a big corrosion rate slope of 35.19 pm/day during Phase 1. Samples #1 and #2 with thermal sprayed composite coatings have a smaller corrosion rate slope of 8.3 and 13.4 pm/day in Phase 1, respectively. This result indicates that the thermal sprayed composite coating used in this study has a higher corrosion resistance when compared with bare steel. To estimate the corrosion related parameters in Equation (6), we take a look at the corrosion rate of Sample #7, the bare steel without coating. The measured corrosion rate of the bare steel using electrochemical method yield to 1.5 mil/year and the corrosion rate slope of the Bragg wavelength change of the embedded FBG is 35.19 pm/day. Thus, the sensitivity of the embedded FBG sensor for corrosion rate measurements, α, can be determined as

$$\alpha = \frac{\mathrm{CR}_7}{s_7} = \frac{1.5\ \mathrm{mil/year}}{35.19\ \mathrm{pm/day}} = 4.26 \times 10^{-2}\ \mathrm{mil{\cdot}day/(pm{\cdot}year)} \quad (13)$$

where s_i stands for the slope of Bragg wavelength change curve of Sample #*i*. Thus, the corrosion rate of Samples #1 and #2 can be calculated as follow:

$$\mathrm{CR}_1 = \alpha \cdot s_1 = 4.26 \times 10^{-2} \times 8.3 = 0.354 \text{ mil/year} \quad (14)$$

$$\mathrm{CR}_2 = \alpha \cdot s_2 = 4.26 \times 10^{-2} \times 13.4 = 0.571 \text{ mil/year} \quad (15)$$

The corrosion rates obtained from the embedded FBG sensors of 0.354 mil/year for Sample #1 and 0.571 mil/year for Sample #2 matches well with the measured corrosion rate of Sample #4 from electrochemical method as in Table 1 of 0.5054 mil/year. Sample #1 showed a smaller corrosion rate than Samples #2 and #4 and a slower start of corrosion process at Day 3 of testing as seen in Figures 14 and 19, indicating a better coating quality.

In Phase 2 (stabilized corrosion progress phase), oxygen starts to diffuse through the corrosion products to further corrode the steel. However, at this phase, oxygen diffuses slower than Phase 1 so the corrosion rate is lower and the amount of corrosion product is in stable. In Figure 19, it is clearly indicated that the corrosion stabilized in this phase with slow Bragg wavelength changes measured from the embedded FBG sensors.

As the corrosion continues and the corrosion product continues to develop, the thermal sprayed coating may crack and release constrains on the embedded sensors, which is required for monitoring its corrosion strain development as discussed in Section 2. In this circumstance, a sudden Bragg wavelength change will be noticed in the embedded FBG sensor reading to show the strain release from the coating to detect corrosion induced cracks in thermal sprayed coatings. In Figure 17, we observed coating crack visually for Sample #4 on Day 3 because the electrochemical method applied on Sample #4 induced serious initial corrosion before the accelerated corrosion tests. A close look at the sensor reading of Sample #4 as in Figure 20, it can be clearly seen that Sample #3 had already passed Phase 0 and Phase 1 and was in Phase 2 when the accelerated corrosion test started. The corrosion induced crack initialization and crack propagation can be clearly identified through dramatic drops of Bragg wavelength of the embedded FBG sensors in seen in Figure 20.

If no corrosion is occurred right on top of the embedded sensor as for Sample #3 shown in Figure 16, the Bragg wavelength of the embedded FBG sensor will stay stable throughout the measurement duration as shown in Figure 21. This phenomenon indicated a limitation of the developed sensor system that it can only measure pit or uniform corrosion of the coatings occurs right at the sensor location, which is a point sensing instead of distributed sensing technique. Future study will be needed to design a reliable sensor network which can cover a reasonable area for corrosion estimation in addition to close range locations.

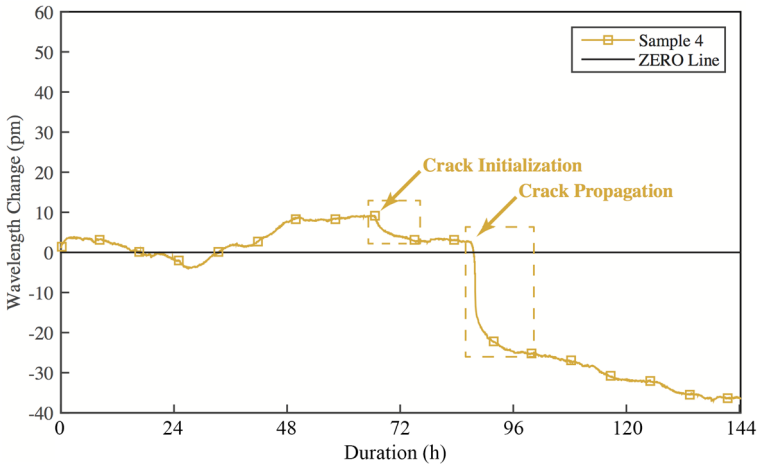

Figure 20. Bragg wavelength change Sample #4 to identify cracks in coating.

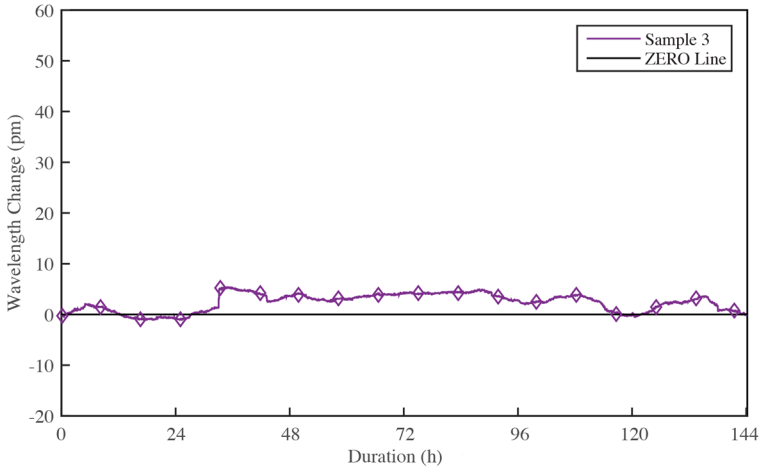

Figure 21. Bragg wavelength change of Sample #3 with no corrosion on top of sensor.

5. Conclusions

In this paper, a corrosion and crack monitoring system was developed for thermal sprayed metallic coatings using embedded FBG sensors. From the results, following conclusions could be drawn:

- A simply supported beam theory can be used to analyze the operational principle of the response of an embedded FBG sensor to corrosion developed in or under coatings.
- The embedded FBG sensors can successfully measure the corrosion progressing of the thermal sprayed coatings and the bare steel through monitoring the Bragg wavelength changes of the FBG sensors.
- Accelerated corrosion tests showed a three-phase phenomenon of the corrosion process of the thermal sprayed composite coatings used in this study and the corrosion rate can be calculated through the slope of Phase 1. The obtained corrosion rate of 0.354 and 0.571 mil/year for thermal sprayed coating matches well with that from the electrochemical method of 0.5054 mil/year.
- The embedded FBG sensors can identify the corrosion induced cracks in coating successfully as shown from the laboratory tests.

To sum up, the laboratory accelerated corrosion tests showed that the developed monitoring system based on embedded FBG sensor showed positive responses on measuring corrosion status, corrosion rate of materials, and crack propagation, which can be further applied for structural assessment and evaluations of metallic coated structural components for a better resource relocation of structural repair and management. Future efforts would be put forward in correlating long-term effect of corrosion to the readings from the embedded FBG sensor and further development of a reliable sensor network which can cover a reasonable area for corrosion estimation in addition to local locations.

Acknowledgments: Financial support to complete this study was provided partially by the U.S. DOT PHMSA under Agreements No. DTPH56-13-H-CAAP05 and No. DTPH56-15-H-CAAP06. The findings and opinions expressed in the paper are those of the authors only and do not necessarily reflect the views of the sponsors.

Author Contributions: Ying Huang conceived and designed the experiments, Fodan Deng performed the experiments and analyzed the data; Farad Azarmi contributed materials coating tools and performed the coating; Yechun Wang provides the equipment and technical assistance for the electrochemical method of the corrosion tests; Fodan Deng and Ying Huang wrote the paper.

Conflicts of Interest: The authors declare no conflict of interest.

References

1. Glass, G.; Page, C.; Short, N. Factors affecting the corrosion rate of steel in carbonated mortars. *Corros. Sci.* **1991**, *32*, 1283–1294. [CrossRef]
2. Southwell, C.; Bultman, J.; Alexander, A. *Corrosion of Metals in Tropical Environments*; Final Report of 16-Year Exposures; National Association of Corrosion Engineers: Houston, TE, USA, 1976.
3. Andrade, C.; Alonso, C. Corrosion rate monitoring in the laboratory and on-site. *Constr. Build. Mater.* **1996**, *10*, 315–328. [CrossRef]
4. Melchers, R.E.; Jeffrey, R. Early corrosion of mild steel in seawater. *Corros. Sci.* **2005**, *47*, 1678–1693. [CrossRef]
5. Bach, F.-W.; Möhwald, K.; Laarmann, A.; Wenz, T. *Modern Surface Technology*; John Wiley & Sons: New York, NK, USA, 2006.
6. Kendig, M.; Scully, J. Basic aspects of electrochemical impedance application for the life prediction of organic coatings on metals. *Corrosion* **1990**, *46*, 22–29. [CrossRef]
7. Sørensen, P.A.; Kiil, S.; Dam-Johansen, K.; Weinell, C. Anticorrosive coatings: A review. *J. Coat. Technol. Res.* **2009**, *6*, 135–176. [CrossRef]
8. Rout, T.; Jha, G.; Singh, A.; Bandyopadhyay, N.; Mohanty, O. Development of conducting polyaniline coating: A novel approach to superior corrosion resistance. *Surf. Coat. Technol.* **2003**, *167*, 16–24. [CrossRef]
9. Hauert, R.; Patscheider, J. From alloying to nanocomposites—Improved performance of hard coatings. *Adv. Eng. Mater.* **2000**, *2*, 247–259. [CrossRef]
10. Matthews, S.; James, B. Review of thermal spray coating applications in the steel industry: Part 1—Hardware in steel making to the continuous annealing process. *J. Therm. Spray Technol.* **2010**, *19*, 1267–1276. [CrossRef]
11. Matthews, S.; James, B. Review of thermal spray coating applications in the steel industry: Part 2—Zinc pot hardware in the continuous galvanizing line. *J. Therm. Spray Technol.* **2010**, *19*, 1277–1286. [CrossRef]
12. Davis, J.R. *Handbook of Thermal Spray Technology*; ASM International: Almere, The Netherlands, 2004.
13. Fauchais, P.; Vardelle, A. *Thermal Sprayed Coatings Used against Corrosion and Corrosive Wear*; INTECH Open Access Publisher: Rijeka, Croatia, 2012.
14. Shibli, S.; Meena, B.; Remya, R. A review on recent approaches in the field of hot dip zinc galvanizing process. *Surf. Coat. Technol.* **2015**, *262*, 210–215. [CrossRef]
15. Tzimas, E.; Papadimitriou, G. Cracking mechanisms in high temperature hot-dip galvanized coatings. *Surf. Coat. Technol.* **2001**, *145*, 176–185. [CrossRef]
16. Szymański, K.; Hernas, A.; Moskal, G.; Myalska, H. Thermally sprayed coatings resistant to erosion and corrosion for power plant boilers—A review. *Surf. Coat. Technol.* **2015**, *268*, 153–164. [CrossRef]
17. Kuroda, S.; Kawakita, J.; Watanabe, M.; Katanoda, H. Warm spraying—A novel coating process based on high-velocity impact of solid particles. *Sci. Technol. Adv. Mater.* **2016**, *9*, 033002. [CrossRef] [PubMed]
18. Mahbub, H. *High Velocity Oxy-Fuel (HVOF) Thermal Spray Deposition of Functionally Graded Coatings*; Dublin City University: Dublin, Ireland, 2005.
19. Toma, D.; Brandl, W.; Marginean, G. Wear and corrosion behaviour of thermally sprayed cermet coatings. *Surf. Coat. Technol.* **2001**, *138*, 149–158. [CrossRef]
20. Guilemany, J.; Fernandez, J.; Delgado, J.; Benedetti, A.V.; Climent, F. Effects of thickness coating on the electrochemical behaviour of thermal spray Cr_3C_2–NiCr coatings. *Surf. Coat. Technol.* **2002**, *153*, 107–113. [CrossRef]
21. Miguel, J.; Guilemany, J.; Mellor, B.; Xu, Y. Acoustic emission study on WC-Co thermal sprayed coatings. *Mater. Sci. Eng. A* **2003**, *352*, 55–63. [CrossRef]
22. Lin, C.-K.; Berndt, C. Measurement and analysis of adhesion strength for thermally sprayed coatings. *J. Therm. Spray Technol.* **1994**, *3*, 75–104. [CrossRef]
23. Steffens, H.-D.; Crostack, H.-A. Methods based on ultrasound and optics for the non-destructive inspection of thermally sprayed coatings. *Thin Solid Films* **1981**, *83*, 325–342. [CrossRef]
24. Rosa, G.; Oltra, R.; Nadal, M.-H. Evaluation of the coating–substrate adhesion by laser-ultrasonics: Modeling and experiments. *J. Appl. Phys.* **2002**, *91*, 6744–6753. [CrossRef]
25. Bescond, C.; Kruger, S.; Lévesque, D.; Lima, R.; Marple, B. In situ simultaneous measurement of thickness, elastic moduli and density of thermal sprayed WC-Co coatings by laser-ultrasonics. *J. Therm. Spray Technol.* **2007**, *16*, 238–244. [CrossRef]

26. Lakestani, F.; Coste, J.-F.; Denis, R. Application of ultrasonic Rayleigh waves to thickness measurement of metallic coatings. *NDT E Int.* **1995**, *28*, 171–178. [CrossRef]
27. Friebele, E.J. Fiber Bragg grating strain sensors: Present and future applications in smart structures. *Opt. Photonics News* **1998**, *9*, 33. [CrossRef]
28. Moyo, P.; Brownjohn, J.; Suresh, R.; Tjin, S. Development of fiber Bragg grating sensors for monitoring civil infrastructure. *Eng. Struct.* **2005**, *27*, 1828–1834. [CrossRef]
29. Guo, Z.-S. Strain and temperature monitoring of asymmetric composite laminate using FBG hybrid sensors. *Struct. Health Monit.* **2007**, *6*, 191–197. [CrossRef]
30. Zhang, B.; Kahrizi, M. High-temperature resistance fiber Bragg grating temperature sensor fabrication. *IEEE Sens. J.* **2007**, *7*, 586–591. [CrossRef]
31. Dewynter-Marty, V.; Ferdinand, P.; Bocherens, E.; Carbone, R.; Beranger, H.; Bourasseau, S. Embedded fiber Bragg grating sensors for industrial composite cure monitoring. *J. Intell. Mater. Syst. Struct.* **1998**, *9*, 785–787. [CrossRef]
32. Betz, D.; Staszewski, W.; Thursby, G.; Culshaw, B. Multi-functional fibre Bragg grating sensors for fatigue crack detection in metallic structures. *Proc. Inst. Mech. Eng. G J. Aerosp. Eng.* **2006**, *220*, 453–461. [CrossRef]
33. Kuang, K.; Cantwell, W.; Thomas, C. Crack detection and vertical deflection monitoring in concrete beams using plastic optical fibre sensors. *Meas. Sci. Technol.* **2003**, *14*, 205. [CrossRef]
34. Kirkby, E.; de Oliveira, R.; Michaud, V.; Manson, J. Impact localisation with FBG for a self-healing carbon fibre composite structure. *Compos. Struct.* **2011**, *94*, 8–14. [CrossRef]
35. Tsuda, H.; Lee, J.-R.; Guan, Y.; Takatsubo, J. Investigation of fatigue crack in stainless steel using a mobile fiber Bragg grating ultrasonic sensor. *Opt. Fiber Technol.* **2007**, *13*, 209–214. [CrossRef]
36. Zheng, Z.; Sun, X.; Lei, Y. Monitoring corrosion of reinforcement in concrete structures via fiber Bragg grating sensors. *Front. Mech. Eng. China* **2009**, *4*, 316–319. [CrossRef]
37. Gao, J.; Wu, J.; Li, J.; Zhao, X. Monitoring of corrosion in reinforced concrete structure using Bragg grating sensing. *NDT E Int.* **2011**, *44*, 202–205. [CrossRef]
38. Hassan, M.R.A.; Bakar, M.H.A.; Dambul, K.; Adikan, F.R.M. Optical-based sensors for monitoring corrosion of reinforcement rebar via an etched cladding Bragg grating. *Sensors* **2012**, *12*, 15820–15826. [CrossRef] [PubMed]
39. Lee, J.-R.; Yun, C.-Y.; Yoon, D.-J. A structural corrosion-monitoring sensor based on a pair of prestrained fiber Bragg gratings. *Meas. Sci. Technol.* **2009**, *21*, 017002. [CrossRef]
40. Hu, W.; Cai, H.; Yang, M.; Tong, X.; Zhou, C.; Chen, W. Fe–C-coated fibre Bragg grating sensor for steel corrosion monitoring. *Corros. Sci.* **2011**, *53*, 1933–1938. [CrossRef]
41. Fontana, M.; Greene, N. *Corrosion Engineering*, 3rd ed.; McGraw-Hill Book Company: New York, NY, USA, 1987.
42. Gangopadhyay, T.K.; Majumder, M.; Chakraborty, A.K.; Dikshit, A.K.; Bhattacharya, D.K. Fibre Bragg grating strain sensor and study of its packaging material for use in critical analysis on steel structure. *Sens. Actuators Phys.* **2009**, *150*, 78–86. [CrossRef]
43. Popov, B.; White, R. Electrochemical and Corrosion Experimental Techniques. Notes USC, Gamry Instruments Technical Report. Available online: https://www.gamry.com/application-notes/corrosion-coatings/basics-of-electrochemical-corrosion-measurements/ (accessed on 22 February 2017).